Biomedical Optics EXPRESS

Full OCT anterior segment biometry: an application in cataract surgery

Sergio Ortiz,[1,*] Pablo Pérez-Merino,[1] Sonia Durán,[2] Miriam Velasco-Ocana,[1] Judith Birkenfeld,[1] Alberto de Castro,[1] Ignacio Jiménez-Alfaro,[2] and Susana Marcos[1]

[1]*Instituto de Óptica "Daza de Valdés", Consejo Superior de Investigaciones Científicas, C/Serrano 121, 28006 Madrid, Spain*

[2]*Fundación Jiménez-Díaz, Avda. Reyes Católicos, 2, 28040, Madrid, Spain*

**sortiz@io.cfmac.csic.es*

Abstract: *In vivo* three-dimensional (3-D) anterior segment biometry before and after cataract surgery was analyzed by using custom high-resolution high-speed anterior segment spectral domain Optical Coherence Tomography (OCT). The system was provided with custom algorithms for denoising, segmentation, full distortion correction (fan and optical) and merging of the anterior segment volumes (cornea, iris, and crystalline lens or IOL), to provide fully quantitative data of the anterior segment of the eye. The method was tested on an *in vitro* artificial eye with known surfaces geometry at different orientations and demonstrated on an aging cataract patient *in vivo*. Biometric parameters CCT, ACD/ILP, CLT/ILT Tilt and decentration are retrieved with a very high degree of accuracy. IOL was placed 400 μm behind the natural crystalline lens, The IOL was aligned with a similar orientation of the natural lens (2.47 deg superiorly), but slightly lower amounts (0.77 deg superiorly). The IOL was decentered superiorly (0.39 mm) and nasally (0.26 mm).

OCIS codes: (110.4500) Optical coherence tomography; (120.6650) Surface measurements, figure; (120.4640) Optical instruments; (120.4800) Optical standards and testing; (110.6880) Three-dimensional image acquisition; (330.7327) Visual optics, ophthalmic instrumentation.

References and links

1. S. Barbero and S. Marcos, "Analytical tools for customized design of monofocal intraocular lenses," Opt. Express **15**(14), 8576–8591 (2007).
2. R. Bellucci and S. Morselli, "Optimizing higher-order aberrations with intraocular lens technology," Curr. Opin. Ophthalmol. **18**(1), 67–73 (2007).
3. S. Norrby, "Sources of error in intraocular lens power calculation," J. Cataract Refract. Surg. **34**(3), 368–376 (2008).
4. T. Olsen, K. Thim, and L. Corydon, "Theoretical versus SRK I and SRK II calculation of intraocular lens power," J. Cataract Refract. Surg. **16**(2), 217–225 (1990).
5. T. Olsen, "Calculation of intraocular lens power: a review," Acta Ophthalmol. Scand. **85**(5), 472–485 (2007).
6. P. R. Preussner, J. Wahl, H. Lahdo, B. Dick, and O. Findl, "Ray tracing for intraocular lens calculation," J. Cataract Refract. Surg. **28**(8), 1412–1419 (2002).
7. J. Tabernero, P. Piers, A. Benito, M. Redondo, and P. Artal, "Predicting the optical performance of eyes implanted with IOLs to correct spherical aberration," Invest. Ophthalmol. Vis. Sci. **47**(10), 4651–4658 (2006).
8. P. Rosales and S. Marcos, "Customized computer models of eyes with intraocular lenses," Opt. Express **15**(5), 2204–2218 (2007).
9. W. Drexler, O. Findl, R. Menapace, G. Rainer, C. Vass, C. K. Hitzenberger, and A. F. Fercher, "Partial coherence interferometry: a novel approach to biometry in cataract surgery," Am. J. Ophthalmol. **126**(4), 524–534 (1998).
10. W. Haigis, B. Lege, N. Miller, and B. Schneider, "Comparison of immersion ultrasound biometry and partial coherence interferometry for intraocular lens calculation according to Haigis," Graefes Arch. Clin. Exp. Ophthalmol. **238**(9), 765–773 (2000).
11. T. Swartz, L. Marten, and M. Wang, "Measuring the cornea: the latest developments in corneal topography," Curr. Opin. Ophthalmol. **18**(4), 325–333 (2007).
12. M. Tang, Y. Li, and D. Huang, "An intraocular lens power calculation formula based on optical coherence tomography: a pilot study," J. Refract. Surg. **26**(6), 430–437 (2010).

#178276 - $15.00 USD Received 19 Oct 2012; revised 26 Dec 2012; accepted 3 Jan 2013; published 31 Jan 2013

13. C. Canovas and P. Artal, "Customized eye models for determining optimized intraocular lenses power," Biomed. Opt. Express **2**(6), 1649–1662 (2011).
14. T. Olsen, "Prediction of the effective postoperative (intraocular lens) anterior chamber depth," J. Cataract Refract. Surg. **32**(3), 419–424 (2006).
15. M. Dubbelman and G. L. Van der Heijde, "The shape of the aging human lens: curvature, equivalent refractive index and the lens paradox," Vision Res. **41**(14), 1867–1877 (2001).
16. P. Rosales and S. Marcos, "Pentacam Scheimpflug quantitative imaging of the crystalline lens and intraocular lens," J. Refract. Surg. **25**(5), 421–428 (2009).
17. P. Artal, S. Marcos, I. Iglesias, and D. G. Green, "Optical modulation transfer and contrast sensitivity with decentered small pupils in the human eye," Vision Res. **36**(22), 3575–3586 (1996).
18. P. Phillips, J. Pérez-Emmanuelli, H. D. Rosskothen, and C. J. Koester, "Measurement of intraocular lens decentration and tilt *in vivo*," J. Cataract Refract. Surg. **14**(2), 129–135 (1988).
19. P. Rosales and S. Marcos, "Phakometry and lens tilt and decentration using a custom-developed Purkinje imaging apparatus: validation and measurements," J. Opt. Soc. Am. A **23**(3), 509–520 (2006).
20. J. Tabernero, A. Benito, V. Nourrit, and P. Artal, "Instrument for measuring the misalignments of ocular surfaces," Opt. Express **14**(22), 10945–10956 (2006).
21. A. de Castro, P. Rosales, and S. Marcos, "Tilt and decentration of intraocular lenses *in vivo* from Purkinje and Scheimpflug imaging. Validation study," J. Cataract Refract. Surg. **33**(3), 418–429 (2007).
22. I. Grulkowski, M. Gora, M. Szkulmowski, I. Gorczynska, D. Szlag, S. Marcos, A. Kowalczyk, and M. Wojtkowski, "Anterior segment imaging with Spectral OCT system using a high-speed CMOS camera," Opt. Express **17**(6), 4842–4858 (2009).
23. I. Grulkowski, J. J. Liu, B. Potsaid, V. Jayaraman, C. D. Lu, J. Jiang, A. E. Cable, J. S. Duker, and J. G. Fujimoto, "Retinal, anterior segment and full eye imaging using ultrahigh speed swept source OCT with vertical-cavity surface emitting lasers," Biomed. Opt. Express **3**(11), 2733–2751 (2012).
24. J. Jungwirth, B. Baumann, M. Pircher, E. Götzinger, and C. K. Hitzenberger, "Extended *in vivo* anterior eye-segment imaging with full-range complex spectral domain optical coherence tomography," J. Biomed. Opt. **14**(5), 050501 (2009).
25. Y. Li, M. Tang, X. Zhang, C. H. Salaroli, J. L. Ramos, and D. Huang, "Pachymetric mapping with Fourier-domain optical coherence tomography," J. Cataract Refract. Surg. **36**(5), 826–831 (2010).
26. M. C. M. Dunne, L. N. Davies, and J. S. Wolffsohn, "Accuracy of cornea and lens biometry using anterior segment optical coherence tomography," J. Biomed. Opt. **12**(6), 064023 (2007).
27. R. Yadav, K. Ahmad, and G. Yoon, "Scanning system design for large scan depth anterior segment optical coherence tomography," Opt. Lett. **35**(11), 1774–1776 (2010).
28. M. Shen, M. R. Wang, Y. Yuan, F. Chen, C. L. Karp, S. H. Yoo, and J. Wang, "SD-OCT with prolonged scan depth for imaging the anterior segment of the eye," Ophthalmic Surg. Lasers Imaging **41**(6 Suppl), S65–S69 (2010).
29. G. Cleary, D. J. Spalton, and J. Marshall, "Anterior chamber depth measurements in eyes with an accommodating intraocular lens: agreement between partial coherence interferometry and optical coherence tomography," J. Cataract Refract. Surg. **36**(5), 790–798 (2010).
30. D. A. Kumar, A. Agarwal, G. Prakash, S. Jacob, Y. Saravanan, and A. Agarwal, "Evaluation of intraocular lens tilt with anterior segment optical coherence tomography," Am. J. Ophthalmol. **151**(3), 406–412.e2 (2011).
31. S. Ortiz, D. Siedlecki, L. Remon, and S. Marcos, "Optical coherence tomography for quantitative surface topography," Appl. Opt. **48**(35), 6708–6715 (2009).
32. S. Ortiz, D. Siedlecki, I. Grulkowski, L. Remon, D. Pascual, M. Wojtkowski, and S. Marcos, "Optical distortion correction in optical coherence tomography for quantitative ocular anterior segment by three-dimensional imaging," Opt. Express **18**(3), 2782–2796 (2010).
33. S. Ortiz, D. Siedlecki, P. Pérez-Merino, N. Chia, A. de Castro, M. Szkulmowski, M. Wojtkowski, and S. Marcos, "Corneal topography from spectral optical coherence tomography (sOCT)," Biomed. Opt. Express **2**(12), 3232–3247 (2011).
34. M. Zhao, A. N. Kuo, and J. A. Izatt, "3D refraction correction and extraction of clinical parameters from spectral domain optical coherence tomography of the cornea," Opt. Express **18**(9), 8923–8936 (2010).
35. K. Karnowski, B. J. Kaluzny, M. Szkulmowski, M. Gora, and M. Wojtkowski, "Corneal topography with high-speed swept source OCT in clinical examination," Biomed. Opt. Express **2**(9), 2709–2720 (2011).
36. S. Ortiz, P. Pérez-Merino, N. Alejandre, E. Gambra, I. Jimenez-Alfaro, and S. Marcos, "Quantitative OCT-based corneal topography in keratoconus with intracorneal ring segments," Biomed. Opt. Express **3**(5), 814–824 (2012).
37. S. Ortiz, P. Pérez-Merino, E. Gambra, A. de Castro, and S. Marcos, "*In vivo* human crystalline lens topography," Biomed. Opt. Express **3**(10), 2471–2488 (2012).
38. S. Ortiz, D. Siedlecki, L. Remon, and S. Marcos, "Three-dimensional ray tracing on Delaunay-based reconstructed surfaces," Appl. Opt. **48**(20), 3886–3893 (2009).
39. S. R. Uhlhorn, D. Borja, F. Manns, and J. M. Parel, "Refractive index measurement of the isolated crystalline lens using optical coherence tomography," Vision Res. **48**(27), 2732–2738 (2008).
40. P. Rosales, M. Wendt, S. Marcos, and A. Glasser, "Changes in crystalline lens radii of curvature and lens tilt and decentration during dynamic accommodation in rhesus monkeys," J. Vision **8**(1), 18 (2008).

#178276 - $15.00 USD Received 19 Oct 2012; revised 26 Dec 2012; accepted 3 Jan 2013; published 31 Jan 2013

41. M. Dubbelman, V. A. Sicam, and G. L. Van der Heijde, "The shape of the anterior and posterior surface of the aging human cornea," Vision Res. **46**(6-7), 993–1001 (2006).
42. M. Dubbelman, G. L. van der Heijde, and H. A. Weeber, "The thickness of the aging human lens obtained from corrected Scheimpflug images," Optom. Vis. Sci. **78**(6), 411–416 (2001).
43. J. C. Merriam, L. Zheng, J. E. Merriam, M. Zaider, and B. Lindström, "The effect of incisions for cataract on corneal curvature," Ophthalmology **110**(9), 1807–1813 (2003).
44. S. Marcos, P. Rosales, L. Llorente, and I. Jiménez-Alfaro, "Change in corneal aberrations after cataract surgery with 2 types of aspherical intraocular lenses," J. Cataract Refract. Surg. **33**(2), 217–226 (2007).
45. B. Lundberg, M. Jonsson, and A. Behndig, "Postoperative corneal swelling correlates strongly to corneal endothelial cell loss after phacoemulsification cataract surgery," Am. J. Ophthalmol. **139**(6), 1035–1041 (2005).
46. Q. Zhang, W. Jin, and Q. Wang, "Repetability, reproducibility, and agreement of central anterior chamber depth measurements in pseudophakic and phakic eyes: optical coherence tomography versus ultrasound biomicroscopy," J. Cataract Refract. Surg. **36**(6), 941–946 (2010).

1. Introduction

Cataract is one of the major causes of vision loss in the aging population, as the crystalline lens progressively loses transparency and opacifies. Upon replacement of the crystalline lens by an intraocular lens (IOL), the source of scattering is eliminated. Current cataract surgery also aims at correcting the refractive errors of the eye, and even optimizing optical quality by reducing high order aberrations. Recently, the customization of IOL design to the anatomical parameters of each patient has been proposed [1,2]. Cataract surgery has advanced considerably with recent improvements in IOL designs, in phacoemulsification (and even all-laser) technologies, and in biometry techniques. However, a limitation to the accuracy of the IOL power selection is the accuracy of pre-operative ocular biometry and the approximations inherent to IOL power calculation formulae [3]. In addition, understanding of performance of current IOL designs, and insights for new IOL designs will definitely benefit from quantitative imaging of the eyes after cataract surgery.

Regression IOL power calculation formulas (such as the SRK or SRK-II) [4] are based on statistical retrospective analysis of post-operative data, although these are decreasingly used today. Theoretical IOL power calculations (i.e., SRK-T) generally use a thin lens approach, and different approximations for the cornea and lens, normally in the paraxial regime [5]. These formulas require at least pre-operative data of axial length and corneal power, as well as estimates of the post-operative anterior chamber depth (ACD), known as Estimated Lens Position (ELP). More recently, the use of exact ray tracing, requiring geometrical and position data of the patient's cornea and lens have been proposed [6]. In fact, custom computer models of eyes implanted with IOLs (including corneal elevation, anterior chamber depth, IOL and ocular alignment) have been shown to predict with high accuracy even the high order aberrations of individual pseudophakic eyes [7,8]. Improved estimates of the Estimated Lens Position, and Custom Eye Models for ray tracing IOL power calculation, as well as for post-operative evaluation of optical performance, require a more complete characterization of ocular geometry than that normally performed clinically, and which is most cases is obtained from multiple instruments.

Improvements in cataract surgery have been paralleled by improvements in biometry techniques. Increasingly used Partial Coherence Interferometry (PCI) for measuring axial length surpasses in resolution A-scan ultrasonography (0.01 vs 0.1 mm) [9,10]. Corneal power is typically measured using keratometry, Placido-based videokeratography, slit-lamp scanning or Scheimpflug imaging [11]. However, the traditional lack of measurements of the posterior corneal surface has led to approximations (i.e., keratometric index) [5], which do not hold in abnormal corneas [12]. In addition, non-paraxial ray tracing approaches would require complete corneal shape information beyond corneal power. Additionally, it is likely that more accurate estimates of the post-operative ELP require more extensive 3-D information of the anterior segment of the eye, and pre-operative crystalline lens. For example, it has been shown that pre-operative ACD correlates with post-operative ACD [13], as well as with lens thickness [14]. A-scan ultrasound, some low coherence interferometry

#178276 - $15.00 USD Received 19 Oct 2012; revised 26 Dec 2012; accepted 3 Jan 2013; published 31 Jan 2013

instruments, and Scheimpflug imaging (provided with distortion correction algorithms [15,16]) offer ACD and lens thickness data, although generally the information provided by commercial instruments is limited to the axial dimension. The alignment of the optical components also plays a role in determining the optical performance in the normal and pseudophakic eye, with impact on coma and astigmatism [17]. Laboratory-based Purkinje-imaging and Scheimpflug imaging methods have been demonstrated and used to measure *in vivo* tilt and decentration of the crystalline lens and IOLs [18–21]. The mechanical stability of the IOL and its alignment in the eye are important factors considered in the design of new IOLs.

Although different imaging techniques are able to quantify biometrical properties of the anterior segment of the eye, currently there is no instrument that provides a full quantitative analysis of the anterior segment geometry, which can be used for planning cataract surgery and for complete assessment of cataract surgery performance.

Spectral Optical Coherence Tomography (sOCT) presents several advantages over other techniques to evaluate ocular anterior segment biometry. It is non-invasive, high-speed, allowing the collection of three dimensional (3-D) anterior segment data in hundreds of milliseconds with high lateral resolution and axial resolution. Recently presented systems with extended axial range even allow capturing the anterior segment of the eye in full [22–24]. Previous studies described the measurement of the geometrical properties of the cornea [25] and lens [26–28] from 3-D OCT images, as well as ACD [29], and tilt in a 2-D cross-sectional OCT image [30]. However, 3-D OCT quantitative geometrical parameters can only be retrieved accurately upon correction of the fan (scanning) and optical (refraction) distortion [31–36]. In addition, automatic image processing tools, which allow accurate segmentation and merging of the different volumes (cornea, iris and lens or IOL) are essential for full biometrical quantification [37].

In this study we demonstrate OCT-based methodologies to estimate 3-D biometrical parameters of the anterior segment of the eye, including interocular distances, as well as tilt and decentration of the lens. The technique is illustrated in an eye with cataract, before and after implantation of an IOL. Along with ocular biometry and alignment, the quantification of the surface topography of the anterior and posterior cornea and anterior and posterior lens previously demonstrated and reported [36,37], the method allows full quantification of the anterior segment of the eye. To our knowledge, this is the first report of 3-D lens alignment measurements with OCT, and of the full *in vivo* anterior segment quantification for a patient before and after cataract surgery.

2. Methods

2.1. Laboratory-based spectral OCT system

Images were collected using a custom-developed spectral OCT system, result of a collaborative effort with Copernicus University [23]. The main features of this system are: 840 nm (50 nm bandwith) SLD illuminating source; spectrometer provided with a 4096-pixel line CMOS camera. The axial range of the instrument is 7 mm, resulting in a theoretical axial pixel resolution of 3.4 μm. The axial resolution predicted by the bandwidth of the SLD laser source is 6.9 μm.

2.2. Validation experiment on in vitro sample

The accuracy of the method to retrieve the shape, tilt and decentration of the lens was tested on an *in vitro* physical model eye. The model eye has been described in prior publications, and also used to validate measurements of IOL tilt and decentration with Purkinje and Scheimpflug imaging [21,32,37]. The water cell model consists of a PMMA cornea and a spherical biconvex IOL with known spherical radii filled with saline solution. The refractive indices of the materials (1.486 for the artificial cornea and the artificial lens, and 1.336 for the

#178276 - $15.00 USD Received 19 Oct 2012; revised 26 Dec 2012; accepted 3 Jan 2013; published 31 Jan 2013

saline solution) were provided by the manufacturers. The lens is mounted on a M-RS40 (Newport corporation, Irvine, CA) manual rotating and x-y translational stage. OCT measurements on the physical model eye were obtained with the SLD power exposure fixed at 800 μW. Each set of 3-D measurements was acquired in 0.72 s with two acquisitions at two different planes of focus (artificial cornea and IOL). The IOL was tilted from −5 to 5 degrees, in 2.5-degree steps. One collection of images was performed at each orientation on a 7x15 mm zone, using 50 B-Scans composed by a collection of 360 A-Scans, providing a resolution of 0.04 mm for horizontal and 0.2 mm for vertical meridian.

2.3. Experiments on a cataract surgery patient

Images were collected on the left eye of a 73 year-old cataract patient before (15 days) and after (90 days) IOL implantation. The study was approved by Institutional Review Boards and followed the tenets of the Declaration of Helsinki. The subject signed a consent form after receiving an explanation of the nature of the study.

Clinical ophthalmological examination and surgery were performed at the Fundación Jiménez-Díaz hospital. A Crystalens AO IOL (Bausch & Lomb Surgical, Aliso Viejo, CA) was implanted through a 2.75-mm corneal incision in the steepest meridian. The IOL power was calculated with the SRK-T formula selecting the closer value to emmetropia (+23.5 D).

Measurements were performed under natural conditions pre-operatively and under mydriasis (phenylephrine 10%) post-operatively. The subject was stabilized using a bite bar. Alignment of the subject was achieved with respect to the anterior corneal specular reflection, while the subject fixated on a reference E-letter target projected on a minidisplay at optical infinity.

A total of 15 sets of 3-D data were collected pre-operatively (3 repeated images for the cornea, anterior lens and posterior lens, respectively), and 9 sets post-operatively (3 repeated images for the cornea and IOL, respectively). All 3-D sets of data contained the iris volume (fixed reference for merging).

The SLD power exposure was fixed at 800 μW. Focus was changed by an automatic displacement system to achieve optimal imaging of the different anterior segment structures (cornea, anterior and posterior lens). In order to minimize the impact of motion artifacts, the image acquisition time was set to 0.72 s. Measurements were collected on a 7x15 mm zone, using 50 B-Scans composed by a collection of 360 A-Scans, providing a resolution of 0.04 mm for horizontal and 0.2 mm for vertical meridian.

2.4. 3-D image analysis

The image processing algorithm can be summarized in 10 steps. The first 9 steps have been described in detail in previous studies [31–33,36–38], and only the new dedicated routines for estimating anterior chamber depth, and 3-D tilt and decentration of the crystalline lens and IOL is described in detail [step (10)].

(1) Denoising: A rotational kernel transform was performed for edge-preserving denoising, using a mask of size 9 pixels. In addition, a wavelet low-pass filtering processing based on log-Gabor wavelet was used for 7 scales and 6 orientations. (2) Statistical thresholding: An adaptive algorithm based on a multimodal Gaussian fitting of the histogram intensity (in a non-linear least squares sense) was performed on the entire 3-D sets of data, which allowed the separation of a noise class from the signal. (3) Volume clustering: the pixels belonging to large volumes representing the objects of interest in 3-D (cornea, iris, anterior crystalline lens surface, posterior crystalline lens surface and IOL) were separated from small volumes through point-connectivity algorithm and thresholding algorithms. (4) Multilayer segmentation: Automatic segmentation was based on Canny detection in each A-scan (1-D signals), following Gaussian (σ = 5 pixels) filtering. (5) Pupil center reference: The pupil center was used as a fixed reference across data sets and to define the optical zone (effective area within the pupil). In the current study, we used the pupil plane in 3-D for

#178276 - $15.00 USD Received 19 Oct 2012; revised 26 Dec 2012; accepted 3 Jan 2013; published 31 Jan 2013

registration and merging. The characteristic vector of the iris plane in all data sets was obtained, which provided the tilt angle of this plane with respect to the OCT coordinate system. (6) 3-D volume merging: Images of the cornea, anterior and posterior lens were merged using the pupil center and pupil plane orientation for registration. In a first step prior to merging, the corneal images were inverted, as, for efficiency in the focus range shift, the cornea was acquired in the opposite side of the Fourier transform (in comparison with the crystalline lens acquisition). The performance of the merging algorithm was tested and described in a previous work [37], showing repeatability in the shapes of the surfaces and in the estimated focal length of the entire within 1% (7) Geometrical distances calculation and further denoising: The registration of the 3-D volumetric data sets involved shift, rotation and resampling using a Delaunay surface description for interpolation. Optical distances were calculated by direct subtraction of the coordinates of the different surfaces, and geometrical distances were obtained by dividing the optical distance by the corresponding group refractive index (1.376 for the cornea, 1.336 for the aqueous humor, 1.403 for the crystalline lens of the subject in the study as per a previously published age-related expression [39], 1.430 for the Crystalens IOL, 1.486 for the PMMA cornea and IOL of the physical model eye, and 1.336 for the saline solution). (8) Fan and optical distortion correction, by propagating the geometrical distances along the directional cosines of each ray, taking into account the refraction that occurs at each interface between media of different refractive indices [32]. (9) Surface fitting to spherical surfaces in a 3-mm diameter optical zone with respect to corresponding surface apex.

(10) Anterior segment biometry: central corneal thickness (CCT), anterior chamber depth (ACD), crystalline lens thickness (CLT), intraocular lens thickness (ILT), intraocular lens position (ILP), and lens IOL tilt (IT) were computed from the corrected 3-D OCT images. CCT is defined as the distance between the anterior and posterior corneal apexes. ACD is defined as the distance between the posterior corneal surface apex and the anterior crystalline lens surface apex. CLT and ILT are defined as the distance between the anterior and posterior lens surface apexes. ILP is defined as the distance between the posterior corneal surface apex and the anterior IOL surface apex. The 3-D Euclidean distances were obtained by direct subtraction of the apexes coordinates obtained from the fittings of the surfaces to spheres,

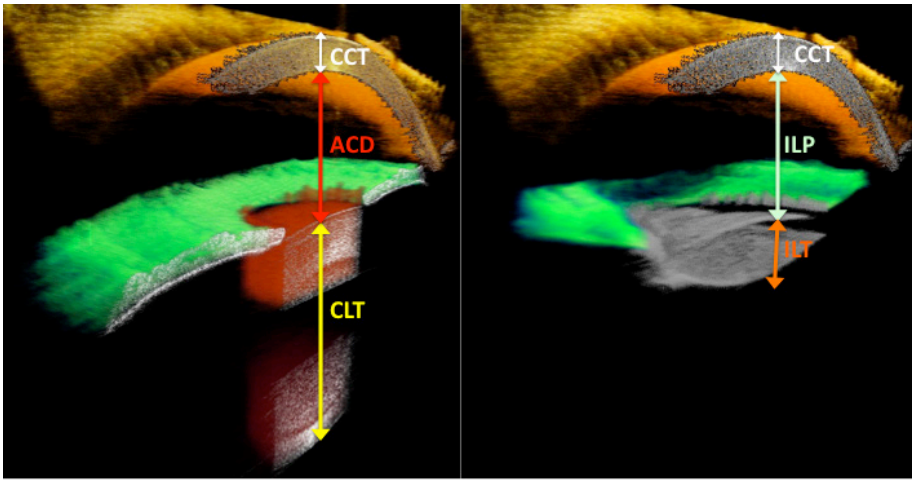

Fig. 1. Illustration of the biometry evaluation from 3-D anterior segment sOCT. (a) Pre-cataract surgery: CCT: Central Corneal Thickness (in white), ACD: Anterior Chamber Depth (in red) and CLT: Central Lens Thickness (in yellow). (b) Post-cataract surgery with IOL implantation: CCT: Central Corneal Thickness (in white), ILP: Intraocular Lens Position (in light green) and ILT: Intraocular Lens Thickness (in orange).

#178276 - $15.00 USD Received 19 Oct 2012; revised 26 Dec 2012; accepted 3 Jan 2013; published 31 Jan 2013

after optical distortion correction. Figure 1 illustrates these definitions, in a 3-D OCT section of the anterior segment in an eye with a natural crystalline lens (prior to cataract surgery)—left panel—and the same eye after IOL implantation—right panel.

Crystalline lens/IOL decentration is defined as the lateral Euclidean distance between the IOL center and the pupil center. Lens tilt is defined as the angle between the axis of the lens and the pupillary axis. The Lens/IOL axis ($\vec{L}$) is defined as the vector that joins the apexes of the anterior and posterior lens surfaces [21]. The pupillary axis ($\vec{P}$) is defined as the vector that joins the center of curvature of the anterior cornea and the pupil center. The angle between axes is obtained by the scalar product of those vectors as it is explained in reference [21]. The horizontal and vertical components of the tilt are obtained, following a sign convention similar to that reported by Rosales et al. [40]. Figure 2 illustrates the crystalline lens (left panel) and IOL (right panel) axes, and the pupilary axis, defining lens tilt.

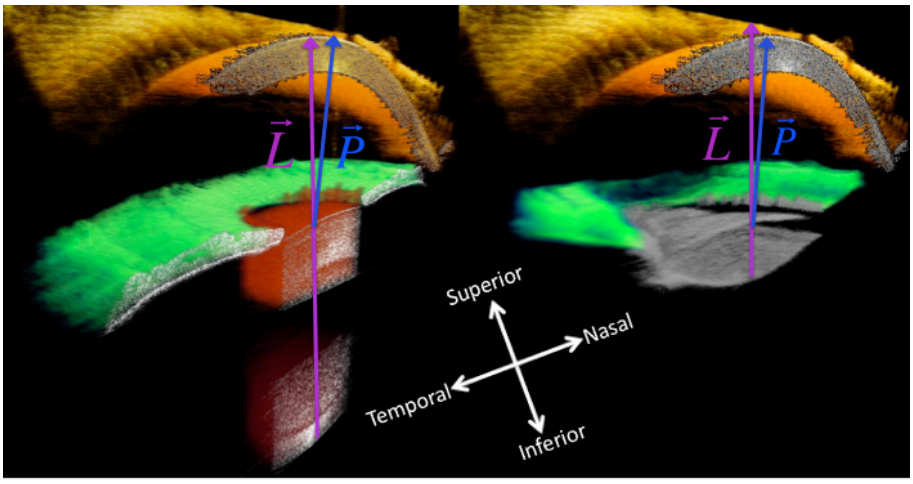

Fig. 2. Illustration of the lens tilt evaluation: Pre-cataract surgery (a), and post-cataract surgery with IOL implantation (b). Vector $\vec{P}$ (in blue) is the pupillary axis, and $\vec{L}$ (in purple) is the Lens/IOL axis.

3. Results

3.1. OCT-based lens tilt measurement: validation on an in vitro physical model eye

The images obtained from the physical model eye were processed using the developed image analysis and distortion correction algorithms. Validation of the retrieved radii of curvature of the artificial cornea and lens, in comparison with nominal data were described in a recent study [37]. Figure 3 shows the measured horizontal tilt values in the physical model eye versus the nominal amount of tilt set in the micrometer stage that holds the lens (varied between −5 and 5 deg). There is an excellent correlation between nominal and measured values, with an average deviation of less than 0.3 deg from nominal values. As expected, the y-axis tilt remains constant through measurements (measured y-axis variations less than 0.31 deg). Slight variations could be associated to manual rotation of the IOL.

#178276 - $15.00 USD Received 19 Oct 2012; revised 26 Dec 2012; accepted 3 Jan 2013; published 31 Jan 2013

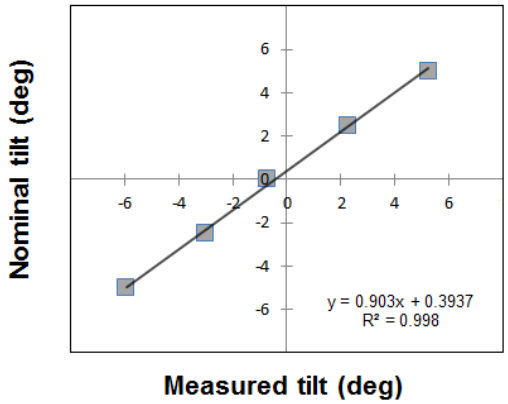

Fig. 3. Comparison of the nominal tilt introduced to the lens of the physical model eye, and the tilt estimated from the OCT images.

3.2. In vivo 3-D anterior biometry: cornea and crystalline lens/IOL

3-D anterior segment biometry (cornea and lens/IOL) is described after full distortion corrections. Radii of curvature of all the surfaces (Table 1) were obtained from sphere fitting. There is a high repeatability in the measurements, both pre and post-operative, and a slight variation in anterior corneal radius of curvature with surgery. There is high measurement repeatability, both across repeated measurements and pre- and post-operative measurements, and 1.2% variation in the anterior radius of curvature (equivalent to a change of 0.58 D in corneal curvature). The anterior corneal astigmatism decreased slightly with surgery (from 0.96 D to 0.63D), while the posterior corneal astigmatism remained fairly constant (0.34 preoperatively and O.31 postoperatively).

Table 1. Radii of curvature of the corneal and crystalline lens/IOL surfaces from sphere fitting

	Radii of curvature (mm)			
	Anterior cornea	*Posterior cornea*	*Anterior lens*	*Posterior lens*
Pre-op (lens)	7.61 ± 0.03	6.82 ± 0.08	8.34 ± 0.25	6.39 ± 0.14
Post-op (IOL)	7.70 ± 0.01	6.80 ± 0.11	6.97 ± 0.06	8.73 ± 0.14

Table 2 shows thickness and interocular distances of the ocular components (CCT, ACD/ILP and CLT/ILT), and tilt and decentration of the crystalline lens/IOL). The anterior surface of the IOL was placed 400 μm behind the natural crystalline lens. CLT is consistent with the average 73-year old lens thickness [41]. Both the crystalline lens and IOL were tilted and decentered with respect to the pupillary axis in the same direction pre- and post-operatively, but their amounts changed significantly with surgery. According to existing conventions [39], negative horizontal decentration stands for nasal (in left eyes), and positive vertical decentration for superior. Positive tilt around the horizontal axis (Tilt x) indicates that the superior edge of the lens is moved forward. Negative tilt around the vertical axis (Tilt y), in left eyes, indicates that the nasal edge of the lens is moved forward.

#178276 - $15.00 USD Received 19 Oct 2012; revised 26 Dec 2012; accepted 3 Jan 2013; published 31 Jan 2013

Table 2. Anterior segment biometry and alignment of the corneal and crystalline lens/IOL

	Anterior segment biometry (mm)						
	CCT (mm)	*ACD/ILP (mm)*	*CLT/ILT (mm)*	*Tilt (x)* (deg)*	*Tilt (y)** (deg)*	*Decentration (x) (mm)*	*Decentration (y) (mm)*
Pre-op (lens)	0.49 ± 0.01	3.14 ± 0.04	4.24 ± 0.05	1.89 ± 0.32	−2.47 ± 0.16	−0.66 ± 0.05	0.17 ± 0.06
Post-op (IOL)	0.47 ± 0.01	3.56 ± 0.10	1.33 ± 0.05	0.04 ± 0.03	−0.77 ± 0.10	−0.26 ± 0.02	0.39 ± 0.07

*Tilt (x) stands for tilt around x-axis (superior/inferior tilt).
**Tilt (y) stands for tilt around y-axis (nasal/temporal tilt).

4. Discussion

We have presented new methodology for 3-D biometry of the anterior segment of the eye based on quantitative OCT, and its application in cataract surgery. 3-D measurements allowed interocular distances and thickness to be measured along the objectively identified axes (as opposed to single A-scan measurements which rely on patient's fixation). In addition, this is, to our knowledge, the first time that the crystalline lens and IOL tilt and decentration have been measured in 3-D using OCT. This information, along with full corneal topography [33,36,37] and axial length measurements, is extremely valuable to improve biometric pre-operative evaluations of cataract surgery, and therefore the selection of the most appropriate IOL design and power, as well as to fully characterize surgical outcomes and optical performance in pseudophakic eyes. In particular, quantitative 3-D OCT anterior segment geometry and biometry will help to improve IOL selection by: (1) providing true corneal power, from anterior and posterior corneal radius of curvature; (2) providing 3-D data for non-paraxial 3-D ray tracing calculations of IOL power calculations and beyond this, full customization of the IOL design; (3) improving accuracy in interocular distances estimations; (4) greatly improving the Estimated Lens Position, which is a key parameter in IOL power calculations [3]. 3-D quantitative views of the full anterior segment of the eye pre- and post-operatively will provide important insights into the pre-operative anatomical parameters affecting the positioning of the implanted IOL beyond the recently explored pre-operative ACD and ILT [14].

The geometrical values retrieved for the patient reported in this study are consistent with previously reported values in the literature. Dubbelman et al. [15,41], using corrected Scheimpflug imaging in a population of 102 subjects of different ages, reported values of corneal radii of curvature [41], and a linear regression of crystalline lens radii of curvature and lens thickness as a function of age [42]. For a 73-year old eye, the predicted radii of curvature from Dubbelman's expression are: 7.79 and 6.53 mm (anterior and posterior cornea), 8.74 and 5.32 mm (anterior and posterior lens), and 4.30 mm for LT, which are very close to the values that we found in this study for a patient of the same age (7.41, 6.82, 8.32, 6.39 and 4.24 mm, respectively). The measured ACD in our patient (3.14 mm) is within the range of values reported in the literature for a similar age (2.87 to 3.80 mm).

Post-operative measurements are interesting to assess possible changes in corneal shape with incision [43]. We found the post-operative anterior cornea to be slightly flatter than the post-operative cornea (1.2%; 0.58D). This was confirmed from Placido disk videokeratography and Scheimpflug imaging in the same patient. There are reports in the literature of changes in corneal curvature with surgery although normally those occur within the first weeks after the surgical procedure and regress with time [43]. Further analysis of the corneal elevation maps, available from OCT, can reveal changes in astigmatism and other high order terms [44]. This patient showed a change in anterior corneal astigmatism (0.33 D). The difference was larger in the vertical meridian, what is consistent with the location of the incision, and similar in amounts to values reports in the literature. The high resolution in axial measurements of CCT, and the high reproducibility with which it can be measured (along

#178276 - $15.00 USD Received 19 Oct 2012; revised 26 Dec 2012; accepted 3 Jan 2013; published 31 Jan 2013

exactly the same axis pre- and post- operatively) revealed small but significant differences in CCT. A slight increase in CCT immediately following surgery could be associated to swelling [45].

Post-operative 3-D biometry reveals interesting features concerning IOL positioning, which are essential to refine estimates of the IOL position (ELP, used in IOL power calculations), and understand the stability of the IOL and its optical performance. ELP depends on individual anatomical parameters (fully available with the reported methodology) and the IOL platform and haptic design. The particular design of the IOL of the example (an accommodating IOL, expected to move axially upon an accommodative effort) may explain the relatively forward position of the lens, and therefore relatively lower post-operative ACD compared to that obtained with common monofocal IOLs (i.e., 3.91 ± 0.28 mm, as obtained for the single-piece aspheric IOL using OCT [46]).

As the IOL design becomes more sophisticated, there is an increasing interest in the assessment of IOL tilt and decentration, and its potential impact on optical quality. Previous studies used Purkinje or Scheimpflug imaging to measure IOL alignment in normal young eyes, and pseudophakic eyes implanted with aspheric monofocal IOLs [7,8,20,21]. In this study, we report for the first time full measurements and validations of IOL tilt and decentration obtained from OCT images. We found amounts and orientations in the natural lens of the patient of study within the range of previous studies [18,19]. In addition, as observed in previous studies, the IOL showed decentration and tilt in the same direction as the natural lens, although the amounts varied slightly. The analysis of the anatomical and IOL design factors (i.e., haptic design) influencing IOL tilt and decentration is interesting for improvement of IOL design parameters.

Customized model eye's using anatomical information for each patient has been shown to provide excellent predictions of wave aberrations (estimated from ray tracing) in pseudophakic eyes, compared to measurements of ocular aberrations performed in the same eye [8]. As cataract surgery heads towards ray-tracing calculations of IOL power, and to customized IOL designs, it becomes more important to obtain accurate biometric parameters. Fully quantitative OCT-based 3-D geometry, and biometry obtained from the same instrument holds promise to become a primary tool in the cataract surgery practice.

5. Conclusions

Anterior segment OCT provided with full distortion correction and automatic analysis tools allowed quantification of the human biometry *in vivo* in 3-D previous and after cataract surgery. The retrieved radii of curvature from OCT, previous operation, agree with phakometric data previously reported using Scheimpflug and Purkinke image along one meridian. Biometric pre and post-operative parameters CCT, ACD/ILP, CLT/ILT Tilt and decentration are retrieved with a very high degree of accuracy. IOL was placed 400 μm behind the natural crystalline lens. In the reported patient the IOL tilt and decentration preserved the orientation of the natural lens (lens tilted with the superior and nasal edge forward, and decentered superiorly and nasally); pre-operative tilt was 3.11 deg and decentration 0.77 mm; post-operative tilt was 0.77 deg and decentration 0.47 mm. OCT-based biometry is a promising tool to investigate the changes after cataract surgery; the contribution of the IOL location and tilt to the overall retinal image quality, and in the design of new IOLs.

Acknowledgments

This study has been funded by Spanish Government Grant FIS2011-25637 and European Research Council Grant ERC-2011-AdG-294099 to S. Marcos. The authors acknowledge the collaborative agreement "Unidad Asociada Tecnología e Innovación sanitaria en Oftalmología" (IIS Fundación Jiménez Díaz/ IO-CSIC).

#178276 - $15.00 USD Received 19 Oct 2012; revised 26 Dec 2012; accepted 3 Jan 2013; published 31 Jan 2013